

# Baryon Resonances in a Chiral Hadronic Model for the QCD Equation of State

Philip Rau,<sup>1, 2,\*</sup> Jan Steinheimer,<sup>1, 2</sup> Stefan Schramm,<sup>1, 2</sup> and Horst Stöcker<sup>1, 3</sup>

<sup>1</sup>*Institut für Theoretische Physik, Johann Wolfgang Goethe-Universität,  
Max-von-Laue-Str. 1, 60438 Frankfurt am Main, Germany*

<sup>2</sup>*Frankfurt Institute for Advanced Studies (FIAS),  
Ruth-Moufang-Str. 1, 60438 Frankfurt am Main, Germany*

<sup>3</sup>*GSI Helmholtzzentrum für Schwerionenforschung GmbH, Planckstr. 1, 64291 Darmstadt, Germany*

In this paper we study the influence of hadronic resonances on the phase diagram calculated with an effective chiral flavour  $SU(3)$  model. We show that varying the couplings of the baryonic resonances to the attractive scalar and the repulsive vector fields has a major impact on the order and location of the chiral phase transition and the possible existence of a critical end point as well as on the thermodynamic properties of the model. Furthermore, we study (strange) quark number fluctuations and show the related susceptibilities both at zero baryochemical potential and when crossing the phase transition line at three different points in the  $T$ – $\mu$  plane. We obtain the best agreement with current lattice data if we choose a rather strong vector coupling which in our model limits the phase transition to a smooth crossover and implies the non-existence of a critical end point.

## I. INTRODUCTION

Currently there are many efforts both on the theoretical, as well as on the experimental side to gain knowledge about the phase diagram of strongly interacting nuclear matter. Experiments with highly energetic colliding gold nuclei at the Relativistic Heavy Ion Collider (RHIC) suggest that a new state of matter, comparable to a nearly perfect fluid, is created at high temperatures [1–4]. While these experiments at RHIC and the Large Hadron Collider (LHC), performed at very high beam energies, aim at the high-temperature, low-density region of the phase diagram, there are also experiments in which higher baryonic densities may be reached, as for example planned at the upcoming Facility for Antiproton and Ion Research (FAIR) at GSI. Common to all these experiments is the search for the phase transition of strongly interacting matter from a confined state of hadrons at low temperatures to a state with deconfined quarks and gluons (QGP) as it is predicted for high densities and high temperatures [5]. This phase transition is commonly referred to as deconfinement transition [6]. The symmetries of quantum chromodynamics (QCD), however, imply another, *chiral* phase transition at which the chiral symmetry is restored and the masses of the baryons, or constituent quarks, vanish [7–9]. For this transition, on which we will mainly focus our studies, the chiral condensate  $\sigma$  acts as the corresponding order parameter.

Since QCD can not be treated perturbatively at low temperatures, most information we have about the phase diagram of QCD matter today comes from lattice QCD calculations [10–19]. In the region of vanishing baryochemical potentials  $\mu = 0$  and finite temperature, lattice QCD yields reliable results that show a smooth crossover transition [15]. For finite potentials  $\mu > 0$ , however, results from lattice QCD are not available because of the

failing of standard Monte Carlo sampling methods due to the so-called sign-problem. Currently there are various methods to extend the lattice results from  $\mu = 0$  to the region of small chemical potentials [11, 12, 20–29]. Some lattice QCD groups suggest that the phase transition becomes first order at a critical endpoint [13, 20, 30–32] with its coordinates varying considerably for different calculations. Other more recent results [33] favour the exclusive existence of a crossover transition for a wide range of baryon densities, implying the non-existence of such a critical point. Moreover, the exact position of the phase transition in the phase diagram is subject of a lively and ongoing debate.

Other common theoretical approaches to QCD are effective models to study specific properties of QCD matter [7, 34–40]. In our approach we will use an effective model for the QCD equation of state to study the properties of the phase diagram of nuclear matter. Our model is able to reproduce the well known saturation properties of nuclear matter [41, 42].

The degrees of freedom in our model are all known baryons and baryonic resonances up to masses of  $m = 2.6$  GeV. This approach resembles an interacting hadron resonance gas (HRG). The HRG is known to give a good description of thermodynamic quantities at low temperatures ( $T \leq T_c$ ) and was often used to reproduce lattice QCD results for thermodynamics and fluctuations of conserved charges at low temperatures [14, 43–48]. The particle production in heavy ion collisions may also be reasonably well described with use of the HRG [49–53]. Therefore, our first approach to use only hadronic degrees of freedom seems to be appropriate up to at least temperatures in the range of  $T_c$ . For higher temperatures, at the latest when the deconfinement phase transition sets in, this approach breaks down and, in a future step, partonic degrees of freedom need to be taken into account as it was done in Refs. [54, 55] for example.

This paper is organised as follows. First we introduce the chiral  $SU(3)$  model in section II. In section III, we

\* rau@th.physik.uni-frankfurt.de

present results for the order parameter of the chiral condensate  $\sigma$  at zero and nonzero baryochemical potentials, thermodynamic quantities from the model, and quark susceptibilities at different points in the phase diagram. Susceptibilities are interesting quantities since they resemble fluctuations of conserved charges which itself are closely linked to phase transitions. They offer an effective possibility of comparison between results from theory and experiment because the susceptibilities can be related to measured fluctuations of particle production. Of particular interest are susceptibility ratios since they are not dependent on the volume or the impact parameter of the underlying system [56]. This work closes with a conclusion in section IV.

## II. MODEL

In our model, a  $SU(3)$ -flavour sigma-omega model using the non-linear realization of chiral symmetry (see Refs. [37, 41, 42, 57] for a comprehensive review), the Lagrangian in mean field approximation has the form

$$\mathcal{L} = \mathcal{L}_{\text{kin}} + \mathcal{L}_{\text{int}} + \mathcal{L}_{\text{meson}}. \quad (1)$$

Here, the first term represents the kinetic energy of the hadrons, the terms

$$\mathcal{L}_{\text{int}} = - \sum_i \bar{\psi}_i (m_i^* + g_{i\omega} \gamma_0 \omega^0 + g_{i\phi} \gamma_0 \phi^0) \psi_i \quad (2)$$

describe the interaction of the baryons with the scalar mesons  $\sigma, \zeta$  (attractive interaction, see Eq. (5)) and the vector mesons  $\omega, \phi$  (repulsive interaction) respectively. The summation index  $i$  runs over the baryon octet ( $N, \Lambda, \Sigma, \Xi$ ), the baryon decuplet ( $\Delta, \Sigma^*, \Xi^*, \Omega$ ), and all heavier resonance states up to masses of  $m_{N^*} = 2600$  MeV. We only include hadronic resonances whose existence is considered to be very likely according to the Particle Data Group listings [58] where they are recorded with a minimum three-star rating. Since the listed masses of some heavy resonances may cover a broad range, all particles are included with their average mass.

The third term of the Lagrangian

$$\begin{aligned} \mathcal{L}_{\text{meson}} &= \mathcal{L}_{\text{vec}} + \mathcal{L}_0 + \mathcal{L}_{\text{ESB}} \quad (3) \\ &= +\frac{1}{2} (m_\omega^2 \omega^2 + m_\phi^2 \phi^2) \\ &\quad + g_4 \left( \omega^4 + \frac{\phi^4}{4} + 3\omega^2 \phi^2 + \frac{4\omega^3 \phi}{\sqrt{2}} + \frac{2\omega \phi^3}{\sqrt{2}} \right) \\ &\quad - \frac{1}{2} k_0 (\sigma^2 + \zeta^2) + k_1 (\sigma^2 + \zeta^2)^2 \quad (4) \\ &\quad + k_2 \left( \frac{\sigma^4}{2} + \zeta^4 \right) + k_3 \sigma^2 \zeta + k_4 \ln \frac{\sigma^2 \zeta}{\sigma_0^2 \zeta_0} \\ &\quad - m_\pi^2 f_\pi \sigma + \left( \sqrt{2} m_k^2 f_k - \frac{1}{\sqrt{2}} m_\pi^2 f_\pi \right) \zeta \end{aligned}$$

includes the self interactions of the vector mesons and the scalar mesons together with the last two terms describing the explicit symmetry breaking.

The effective masses of the baryons

$$m_i^* = g_{i\sigma} \sigma + g_{i\zeta} \zeta + \delta m_i \quad (5)$$

are created by the coupling of the baryons to the scalar meson fields (i.e. the non-strange chiral condensate  $\sigma$  and its strange equivalent  $\zeta$ ), together with an explicit mass of at least  $\delta m_N = 150$  MeV. In this way at high temperatures and baryonic densities the decreasing  $\sigma$ -field leads to smaller baryon masses and thus to the restoration of chiral symmetry. Thereby the nucleons which have the smallest explicit mass have lost roughly 45% of their vacuum mass at  $T_c$ . Since our model only includes hadronic degrees of freedom it can only be applied in the hadronic regime up to temperatures slightly above  $T_c$ . This also prevents baryonic masses from getting to small so that the mean field approximation should remain valid and no fluctuations need necessarily to be taken into account as it was for example done in Refs. [59, 60].

The effective masses of the pseudoscalar mesons and vector mesons are given by the second derivative of the mesonic potential  $\mathcal{V}_{\text{meson}} = -\mathcal{L}_{\text{vec}} - \mathcal{L}_0 - \mathcal{L}_{\text{ESB}}$  with respect to the respective mesons  $\xi_j$  at the minimum of the grand canonical potential (see Eq. (9)) [61]

$$\begin{aligned} m_j^* &= \frac{\partial^2}{\partial \xi_j^2} \mathcal{V}_{\text{meson}}(\xi_j^0), \quad (6) \\ \xi_j &= \pi, \eta, \eta', K, \bar{K}; \rho, \omega, \varphi, K^*, \bar{K}^*. \end{aligned}$$

The couplings of the baryon octet to the mesonic fields and the mesonic potential are chosen in such a way as to reproduce the well-known vacuum masses, the nuclear ground state properties (e.g. the correct binding energy), and the asymmetry energy. The coupling strengths of the baryons of the decuplet and all heavier resonances are scaled to the nucleon couplings via the parameters  $r_s, r_v$  according to

$$g_{B\sigma,\omega} = r_{s,v} \cdot g_{N\sigma,\omega}, \quad (7)$$

$$g_{B\zeta,\phi} = r_{s,v} \cdot g_{N\zeta,\phi}. \quad (8)$$

In this paper we systematically analyse the influence of the baryonic resonances on the hadronic matter properties. Therefor we adjust the vector coupling parameter  $r_v$ , controlling the abundance of the baryonic resonances at finite baryochemical potentials in the model, in order to study the influence on the resulting phase diagram and the thermodynamic properties of the model. We use this one-parameter approximation in order not to be swamped by a plethora of unknown coupling constants of the various hadronic multiplets. In this work we set the scalar coupling parameter fixed to  $r_s = 0.97$  which ensures a smooth crossover phase transition at zero baryochemical potential (see Fig. 1 (b) for a study of the effect of  $r_s$ ). In general the scalar couplings are fixed by

reproducing the particles' vacuum masses (except for the explicit mass term  $\delta m_i$ ).

As a reference we also perform calculations for an ideal HRG that is not interacting with the mesonic fields. In this particular case all baryon couplings to the fields  $g_B$  are set to zero and the masses of all particles are fixed at their tabulated vacuum expectation value.

The grand canonical potential of our model takes the form

$$\frac{\Omega}{V} = -\mathcal{L}_{\text{int}} - \mathcal{L}_{\text{meson}} + \Omega_{\text{th}} \quad (9)$$

with the thermal contribution of the hadrons in the model

$$\begin{aligned} \Omega_{\text{th}} = & -T \sum_{i \in B} \frac{\gamma_i}{(2\pi)^3} \int d^3k \left( \ln \left[ 1 + e^{-\frac{1}{T}(E_i^*(k) - \mu_i^*)} \right] \right. \\ & \left. + \ln \left[ 1 + e^{-\frac{1}{T}(E_i^*(k) + \mu_i^*)} \right] \right) \quad (10) \\ & + T \sum_{j \in M} \frac{\gamma_j}{(2\pi)^3} \int d^3k \ln \left[ 1 - e^{-\frac{1}{T}(E_j^*(k) - \mu_j)} \right]. \end{aligned}$$

Here the sums run over all baryons  $B$  (anti baryons are explicitly included in the second term of the first integral) and all mesons  $M$  in the model,  $\gamma_{i,j}$  stands for the spin-isospin-degeneracy factor of the respective particle species  $i, j$  and  $E_{i,j}^*(k) = \sqrt{k^2 + m_{i,j}^{*2}}$  for the single particle energies. The effective baryochemical potential is defined as  $\mu_i^* = \mu_i - g_{i\omega}\omega - g_{i\phi}\phi$ . The grand canonical potential then leads to the thermodynamic quantities of the system, i.e. the pressure  $p$  and the energy and entropy density  $e, s$ , together with the densities of the particular particle species  $\rho_i$ .

Another effect we include in our model (following the works of Refs. [55, 62]) is the effective suppression of baryonic states at high densities due to excluded volume effects [63–66]. While so far all particles were regarded as point like, we now can introduce for every single particle  $j$  an average finite volume  $v_{\text{ex}}^j$  excluded from the total volume of the system  $V$ . In a first and very basic consideration this excluded volume in a non-relativistic definition takes the form

$$v_{\text{ex}}^j = \frac{1}{2 a_i} \frac{4}{3} \pi (2r)^3, \quad (11)$$

where  $r$  is the mean radius of all particles in the model and the parameter  $a_i$  defines the excluded volume for the different particle species  $i$ . In our case we set  $a_{B,M} = 1$  as a first approximation for all baryons and mesons. This modification leads to the altered chemical potential

$$\mu'_j = \mu_j - v_{\text{ex}}^j P, \quad (12)$$

where  $P$  is the sum over all partial pressures. All thermodynamic observables must now be expressed in terms of  $T$  and  $\mu'_j$ . Furthermore, a volume correction factor for each particle species

$$f_i = \frac{V'_i}{V} = \left( 1 + \sum_j v_{\text{ex}}^j \rho_j \right)^{-1} \quad (13)$$

with  $V'_i$  the volume not being occupied, has to be introduced in order to express the densities in a thermodynamically consistent way

$$\rho'_i = f_i \rho_i, \quad (14)$$

$$e' = \sum_i f_i e_i, \quad (15)$$

$$s' = \sum_i f_i s_i. \quad (16)$$

The inclusion of the excluded volume effects also has an impact on the nuclear ground state properties and thus this approach is considered only as a first attempt to study the impact of the suppression of baryons on the phase transition and on the thermodynamic properties of the model. However, reasonable nuclear ground state properties can be achieved by recalibration of the parameters as it was shown in Ref. [67].

### III. RESULTS

#### A. Order Parameters

We start our investigation of the model properties with the calculation of the order parameter for the chiral transition  $\sigma$  at zero baryochemical potential  $\mu_B$ . Figure 1 (a) shows the normalised chiral order parameter as a function of the temperature together with data from lattice QCD calculations. Here and in the following, the lattice data we refer to were obtained by different collaborations using various lattice actions (asqtad, hisq, p4 and stout) and temporal spacings of the lattice ( $N_\tau = 4 - 12$ ) [33, 46, 48, 68–73].

With the scalar couplings fixed to  $r_s = 0.97$  we obtain a smooth crossover in  $\sigma$  for both the model with excluded volume (green dashed line) effects due to finite size of the particles and without it (red solid line). The critical temperature, defined as the point with the largest increase in  $\sigma$ , is found to be  $T_c = 164$  MeV without the excluded volume effect and  $T_c = 174$  MeV if the finite size effects are taken into account. The results for  $\sigma$  without the excluded volume effects are in qualitatively good agreement with lattice QCD calculations which predict a smooth crossover at  $\mu_B = 0$  and critical temperatures in the range from  $T_c = 155$  MeV to 200 MeV [15, 33, 46, 68–72, 75], where the newest continuum extrapolated data from the Hot-QCD and the Wuppertal-Budapest Collaborations predict critical temperatures close to  $T = 160$  MeV consistently. For temperatures below  $T_c$  the slope of the chiral condensate from our model is relatively steep and deviates from those suggested by lattice QCD calculations. This is mainly due to neglecting contributions from pseudoscalar meson self interactions which are important at low temperatures [76]. The slope of  $\sigma$  could be leveled by including the  $\pi$  self interaction in the model [67, 77].

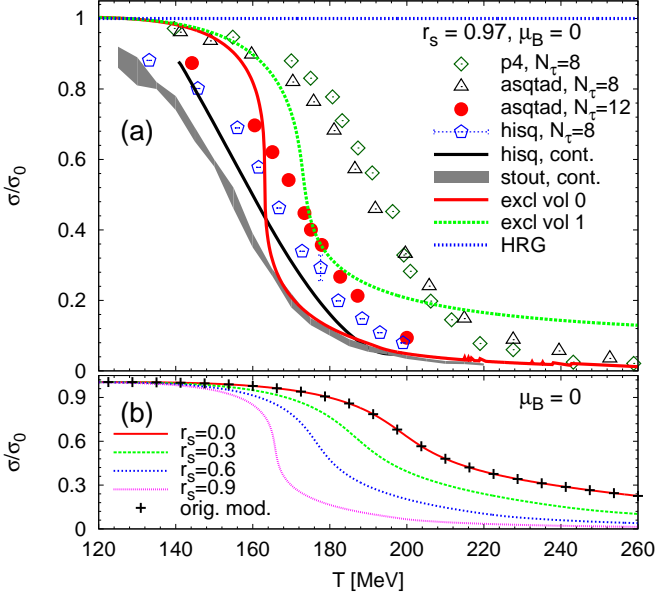


Figure 1. (Color online) (a) Normalised order parameter for the chiral condensate  $\sigma/\sigma_0$  as a function of  $T$  at  $\mu_B = 0$  with (green dotted line) and without (red solid line) excluded volume corrections compared to lattice data. The blue dotted line at  $\sigma/\sigma_0 = 1$  shows the reference line of the non-interacting ideal hadron resonance gas. Here and in the following plots the lattice data are shown as calculated with the asqtad [68], the hisq [69, 70], the p4 [48, 68, 71], and the stout action [46, 72, 74] on lattices with different temporal extent  $N_\tau$ . Panel (b) shows  $\sigma/\sigma_0$  for different strength of the scalar coupling  $r_s$  together with results from our model without any resonance states.

The impact of the heavy resonance states can be seen from Fig. 1 (b) where the black dots show the normalised chiral order parameter as a function of the temperature as calculated with our original model which does not include any hadronic resonance states [41, 42]. It shows that without the hadronic resonance states the transition is much smoother and exhibits a higher critical temperature close to  $T_c = 200$  MeV. The same effect is achieved by decreasing the strength of the attractive coupling of the baryons to the scalar  $\sigma$ -field. This behavior is also shown in Fig. 1 (b) for values of  $r_s$  from 0 to 0.9. The weaker the scalar coupling is, the flatter is the transition and the critical temperature moves to higher temperatures. For vanishing scalar couplings (red line) the results are the same as in the original model. Note that for small values of  $r_s$  one would have to introduce large values for the explicit mass term as the sum of the meson-field generated mass and the explicit term have to reproduce the vacuum masses of the states.

Next we extend this study of  $\sigma$  to nonzero baryochemical potentials, i.e. the whole  $T-\mu_B$  plane. One of the major interests in the study of the phase diagram of strongly interacting matter is certainly to obtain information about the chiral and deconfinement phase transitions and the search for a possible critical end point which

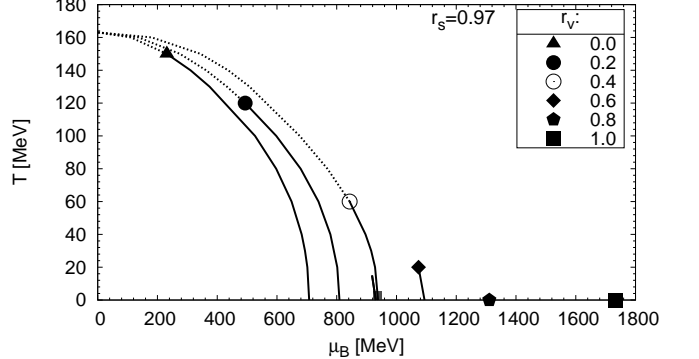


Figure 2. Phase transition lines of the chiral order parameter  $\sigma$  in the  $T-\mu_B$  plane for different values of  $r_v$  together with the nuclear ground state at  $\mu_B = 939$  MeV,  $T = 0$  and the liquid gas first order phase transition. The point on each phase transition line depicts the critical end point, separating a first order phase transition (solid lines) from a crossover (dotted lines). Note that for values  $r_v > 0.6$  there is solely a very broad crossover in the whole  $T-\mu_B$  plane.

divides the crossover phase transition at vanishing baryochemical potential from a first order phase transition at finite chemical potentials. Since lattice QCD calculations are systematically limited to  $\mu_B = 0$  due to the so-called sign problem, different lattice QCD groups use various methods to extend their results to non-vanishing potentials. Unfortunately, this did not lead to a consistent picture for the critical end point until now. While results from (2+1)-flavour QCD calculations suggested the critical end point at a critical quark chemical potential in the range from  $\mu_B^{\text{crit}} \approx 725$  MeV [20] to  $\mu_q^{\text{crit}} \approx 140$  MeV [73] (with  $3\mu_q = \mu_B$ ) and  $\mu_B^{\text{crit}} \approx 360$  MeV [13], more recent studies of the Wuppertal-Budapest Collaboration [33] doubt the existence of a critical end point at all and suggest a broad crossover phase transition over the whole  $T-\mu_B$  plane.

In Fig. 2 we show the results from our model without excluded volume effects for different values of the coupling constant of the repulsive vector interaction  $r_v$ . In this figure the lines represent the biggest increase of the  $\sigma$ -field when varying  $T$  and  $\mu$ . While a discontinuous first order phase transition in  $\sigma$  is depicted by a solid line, a smooth crossover in  $\sigma$  is drawn with a dotted line. The point on each phase transition line stands for the critical end point for the specific choice of  $r_v$ . We find that increasing the vector coupling strength leads to a stronger suppression of heavier particles and thus to a phase transition at higher chemical potentials. Note that for all coupling strengths smaller than  $r_v = 0.4$  the nuclear ground state at  $\mu_B = 939$  MeV,  $T = 0$  and the first order liquid gas phase transition are located above the phase boundary in the chirally restored phase. Therefore, within our simple model approximations those small vector couplings do not lead to physically reasonable solutions. Thus, we conclude according to our model the smallest critical chemical potential (for  $r_v = 0.4$ ) is lo-

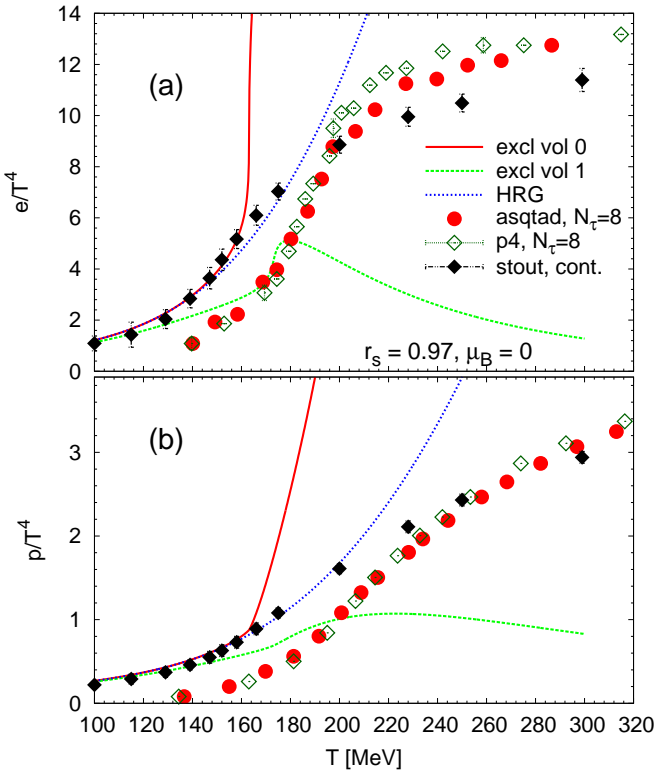


Figure 3. (Color online) Energy density (a) and the pressure (b) divided by  $T^4$  at  $\mu_B = 0$  as a function of the temperature. Depicted are results for the interacting hadronic gas with (green dashed line) and without (red solid line) excluded volume corrections and for the non-interacting ideal hadron resonance gas (blue dotted line) together with lattice data.

cated at  $\mu_B^{\text{crit}} \approx 840$  MeV which is two times higher than the value suggested in Ref. [73].

For vector couplings of  $r_v = 0.6$ , in our model, there is a very small temperature range of first order phase transition going up to  $T^{\text{crit}} \approx 20$  MeV, at higher temperatures there is a broad-ranged crossover transition. For all higher vector couplings, the first order phase transitions vanish completely and only a broad crossover region remains.

## B. Thermodynamics

The thermodynamic quantities, as predicted by our model at  $\mu_B = 0$  are depicted in Fig. 3. Panel (a) shows the energy density and panel (b) shows the pressure both divided by  $T^4$ , in comparison to lattice data. Here and in the following plots, the solid red curve represents the results from our regular model including all baryonic resonances, the green dashed curve depicts the results from the model with the excluded finite size volume effects taken into account and the blue dashed line stands for the non-interacting ideal HRG without finite size effects.

For the standard case in our model, at  $T_c$  the energy

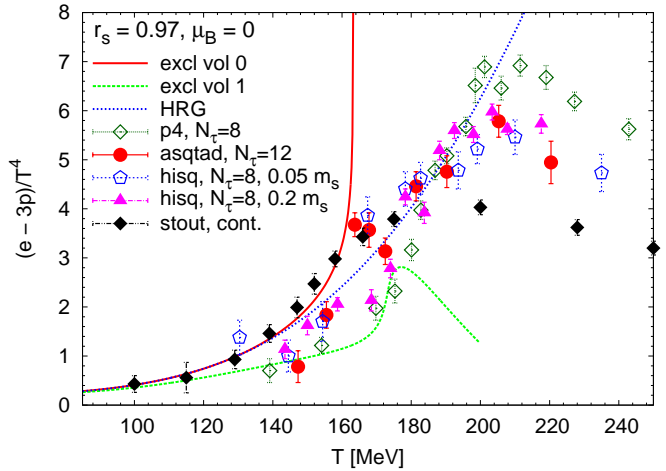


Figure 4. (Color online) The interaction measure, three times the pressure subtracted from the energy density over  $T^4$ , as a function of the temperature at  $\mu_B = 0$  for the interacting hadronic gas with (green dashed line) and without (red solid line) excluded volume corrections and for the non-interacting ideal hadron resonance gas (blue dotted line) compared to lattice data [19, 46, 48, 68, 69, 71, 72, 74, 78]. The data for the hisq action is shown for two different values of the light quark mass  $m_l = 0.05 m_s$  and  $0.20 m_s$ , where  $m_s$  stands for the strange quarks mass.

density and the pressure rise rapidly due to the emerging abundance of particles in the system because of their decreasing masses. Besides a slightly higher critical temperature, the suppression of heavier particles caused by the finite size effects leads to a much smaller maximum of the energy density at  $T_c$  and a decrease for higher temperatures. In this case, three times the pressure divided by  $T^4$  exhibits only a slight increase with a maximum around  $T_c$  and decreases smoothly again for higher temperatures. The HRG results rise monotonically, as expected.

Figure 4 shows the so-called interaction measure defined as the energy density minus three times the pressure divided by  $T^4$  as a function of the temperature. Again, the results from our regular model (red curve) show a rapid increase of this quantity at  $T_c$ , the HRG rises monotonously being in qualitatively good agreement in the region around the critical temperature with lattice data [48, 68, 71] which shows a peak slightly above  $T_c$ .

Comparing our results for the thermodynamic quantities to lattice data, we state that a good agreement up to the critical temperature is achieved for our results from the interacting HRG without excluded volume effects and the continuum extrapolated stout action with physical quark masses. However, for temperatures even below the critical temperature, we overshoot the results from all other lattice actions.

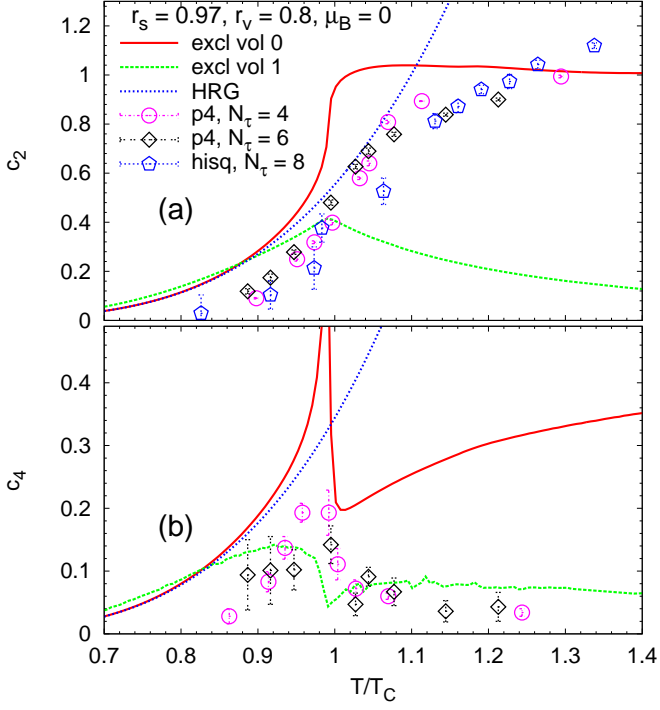


Figure 5. (Color online) Second order (a) and fourth order (b) quark number susceptibilities as a function of  $T/T_c$  at  $\mu_B = 0$ . Results for the interacting hadronic gas ( $r_v = 0.8$ ) with (green dashed line) and without (red solid line) excluded volume corrections and for the non-interacting ideal hadron resonance gas (blue dotted line) are shown compared to lattice data [45, 48].

### C. Susceptibilities

As mentioned above, lattice QCD calculations are largely restricted to zero chemical potential because of the sign problem. However, thermodynamic quantities at non-vanishing potentials may be obtained by Taylor expansion methods as described in Refs. [22, 48, 73, 79].

The pressure at a specific point in the phase diagram  $p(T, \mu_B)$  with preferably small chemical potentials is calculated by expanding the pressure at  $p(T, \mu_B = 0)$  around  $\mu_B/T$

$$\frac{p(T, \mu_B)}{T^4} = \sum_{n=0}^{\infty} c_n(T) \left( \frac{\mu_B}{T} \right)^n \quad (17)$$

with the Taylor coefficients

$$c_n(T) = \frac{1}{n!} \left. \frac{\partial^n (p(T, \mu_B)/T^4)}{\partial (\mu_B/T)^n} \right|_{\mu_B=0} . \quad (18)$$

The coefficients  $c_n(T)$  are proportional to the quark number susceptibilities reflecting quark number fluctuations [80].

Similarly, by expanding the pressure with respect to the strange chemical potential  $\mu_s$ , the first order strange

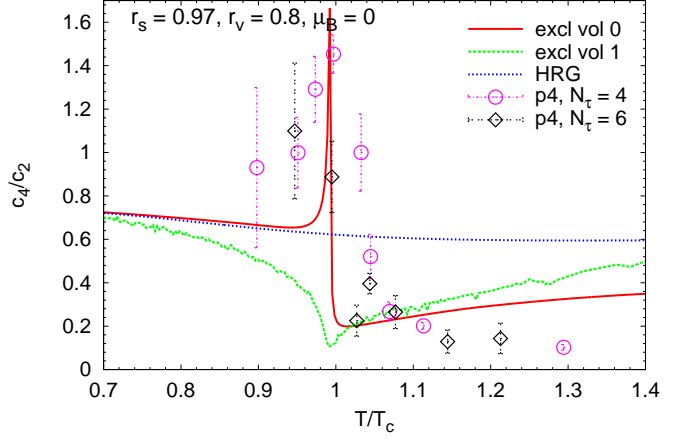


Figure 6. (Color online) Ratio of the fourth order to the second order quark number susceptibility as a function of  $T/T_c$  at  $\mu_B = 0$  for the three different cases as described in Fig. 5 together with lattice data [48, 68, 71, 73].

quark susceptibility  $\chi_s(T)$  can be found to be

$$\chi_s(T) = T^2 \left. \frac{\partial^2 (p(T, \mu_s))}{\partial \mu_s^2} \right|_{\mu_s=0} . \quad (19)$$

In contrast to lattice QCD, with our model we are able to calculate the pressure at any point in the phase diagram and can therefore numerically calculate the corresponding susceptibilities.

In Fig. 5 we show the second order  $c_2$  (a) and fourth order  $c_4$  (b) quark number coefficients in comparison to lattice QCD data [48, 68, 71, 73] at  $\mu_B = 0$ . Both, the model with and without the excluded volume effects show a maximum of  $c_2$  at the critical temperature and a smooth decrease for higher temperatures. The fourth order coefficient  $c_4$  exhibits a narrow peak at  $T_c$ . As expected, the ideal non-interacting HRG susceptibilities do not show any peak due to the absence of a phase transition. The susceptibilities of the ideal HRG come closest to the lattice data with the  $p4$ -action. However, a comparison to the not yet available susceptibilities from the continuum extrapolated stout action would be very interesting since the lattice results with the stout action gives the best agreement for the thermodynamic quantities and the strange quark susceptibility (Fig. 7).

In our study, we found that the strength of the repulsive vector coupling has a major influence on the extent of the fluctuations at the phase transition, even though the derivative is performed at  $\mu_B = 0$ . This effect was already pointed out in Refs. [81, 82]. A lower vector repulsion leads to significantly higher fluctuations of conserved charges at  $T_c$ . In our study we set the vector coupling to  $r_v = 0.8$  in order to match our results with lattice data up to  $T \approx T_c$ . This vector coupling strength stands in contradiction to the one we found earlier to be suitable to reproduce a critical end point in the region suggested by lattice QCD results ( $r_v \leq 0.2$ , cf. Fig. 2).

In Fig. 6 we show the ratio of the fourth order to the

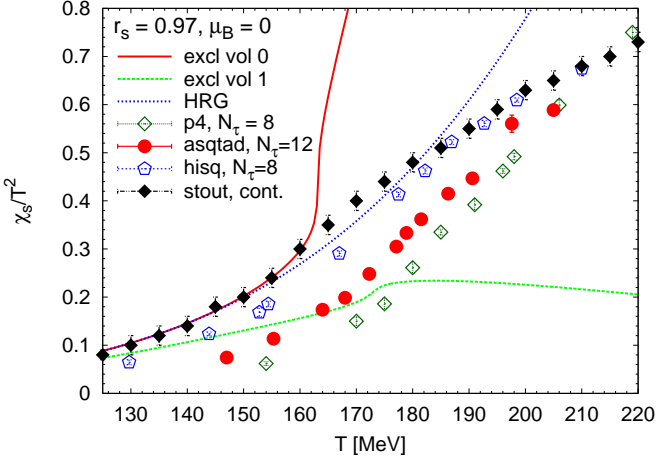


Figure 7. (Color online) Strange quark number susceptibility divided by  $T^2$  at  $\mu_B = 0$  as a function of  $T$  for the three different cases as described in Fig. 5 together with lattice data [33, 46, 69, 70, 72]. The vector coupling strength is set to  $r_v = 0$ .

second order baryon number susceptibility. For the regular model without finite size corrections the ratio is in line with the completely flat curve of the HRG up to the critical temperature. The curve exhibits a discontinuity at  $T_c$  with a sudden decrease above. For higher temperatures the curve is mostly constant around  $c_4/c_2 \approx 0.3$ . Due to the effective suppression of degrees of freedom at the phase transition, the results with excluded volume effects have a significantly different shape with a much smoother curve showing only a minimum peak at  $T_c$ .

The strange quark number susceptibility  $\chi_s$  divided by  $T^2$  is shown in Fig. 7. Again, the three cases of our model yield significantly different results. The curve for the non-interacting ideal HRG rises again monotonically as expected. The regular model with all interactions switched on shows a massive rise at  $T_c$ . The results from our interacting model is once again in good agreement with results from lattice QCD with the continuum extrapolated stout action up to temperatures of  $T_c$ . In the case with the excluded volume effects, in particular heavy strange particles are suppressed and thus the curve is much lower in this case showing a maximum at  $T_c$  and a slow decrease for higher temperatures.

In a next step we study the susceptibility coefficients at non-zero baryochemical potentials. Therefore, we compare the coefficients in three different regions of the phase diagram, namely in the crossover region, at the critical end point, and at the first order phase transition. For this purpose, in a first attempt we set the vector coupling to  $r_v = 0$ , because this leads to a clearly observable and well defined phase transition line and a critical end point at  $\mu_B^{\text{crit}} \approx 220$  MeV; later on we will also calculate susceptibilities with more realistic and stronger vector couplings. Note, that for higher values of  $r_v$  this subdivision of the phase diagram into three clearly distinguishable regions no longer applies. For a vector coupling strength

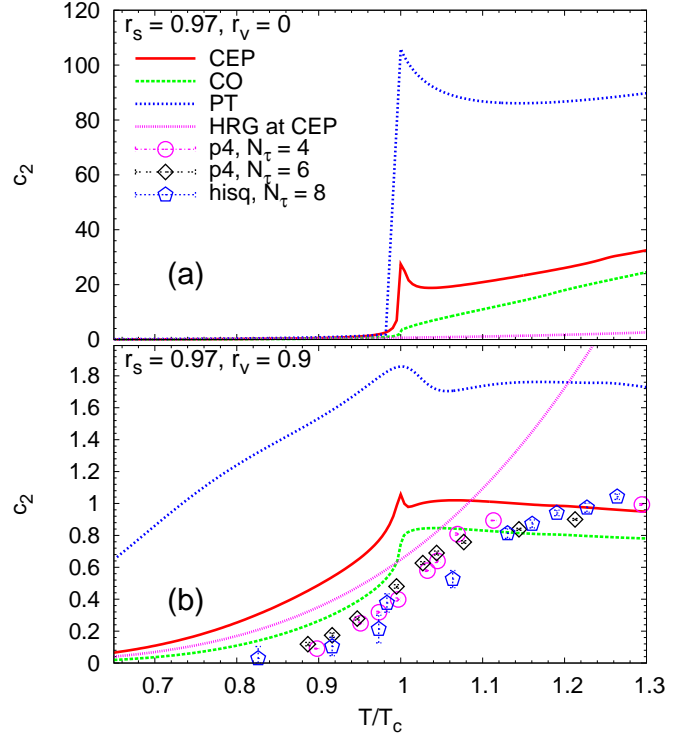


Figure 8. (Color online) Second order quark number susceptibilities  $c_2$  for vector couplings  $r_v = 0$  (a) and  $r_v = 0.9$  (b). The quantities are calculated going perpendicularly through the phase transition line at three different points with  $\mu_B \neq 0$ . For  $r_v = 0$  the blue line depicts the crossing of the phase boundary in the first order phase transition regime, the green line in the crossover regime, and the red line shows  $c_2$  going directly through the critical end point (see text for more information). Shown is also the reference of the ideal hadron resonance gas at the critical end point and lattice data at  $\mu_B = 0$  [48, 68, 71, 73].

of  $r_v > 0.6$ , our model exhibits only a broad crossover transition in the whole  $T-\mu_B$  plane (cf. Fig. 2).

With our model we then calculate the second and fourth order susceptibilities along straight lines perpendicular to the phase boundary going through the points on the phase transition line  $\mu_B^{(1)} = 29.3$  MeV,  $T^{(1)} = 161.7$  MeV for the crossover region,  $\mu_B^{(2)} = 216.0$  MeV,  $T^{(2)} = 150$  MeV at the critical end point, and  $\mu_B^{(3)} = 489.0$  MeV,  $T^{(3)} = 105$  MeV for the first order phase transition region.

In Fig. 8 we show the second order coefficients for the three different regimes for  $r_v = 0$  in panel (a) and for  $r_v = 0.9$  in panel (b), together with lattice data [48, 68, 71, 73] calculated at vanishing baryochemical potential  $\mu_B = 0$ . Note, that choosing a vanishing vector coupling of the baryon resonances leads to unreasonably high susceptibilities at  $T_c$  and must be regarded as a limiting test case. The green dashed curve shows the susceptibilities in the crossover region at low  $\mu_B$ . Due to the smooth transition of the quantities, the susceptibility only shows a small

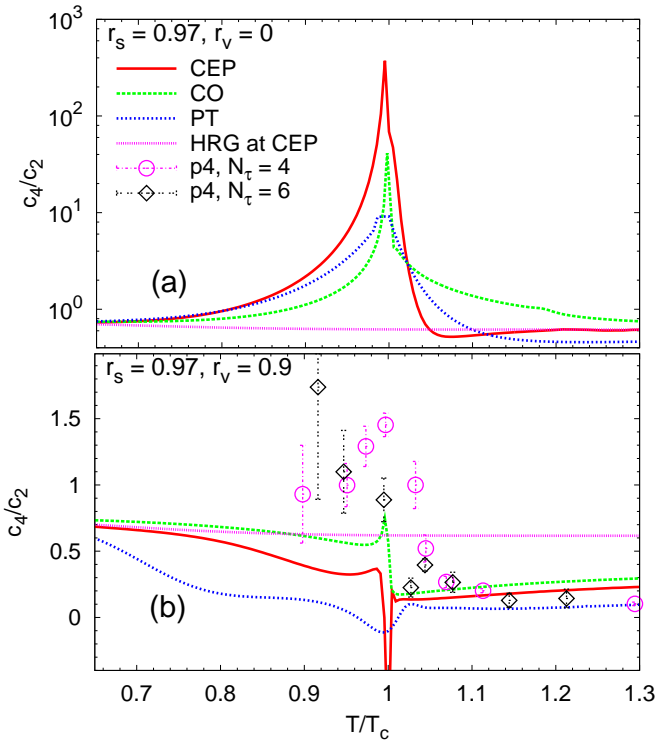


Figure 9. (Color online) Ratios of the fourth order to the second order quark number susceptibilities for vector couplings  $r_v = 0$  (a) and  $r_v = 0.9$  (b) at different regimes of the phase diagram. The line styles are as described in the previous figure. Please note the logarithmic scale in the upper panel (a).

maximum (rise) at  $T_c$  for  $r_v = 0.9$  ( $r_v = 0$ ). The susceptibilities at the discontinuous first order phase transition (blue dashed line) show the highest maximum for both values of  $r_v$ , as expected. At the critical end point (red solid line), the maximum of  $c_2$  is located in between the results from the crossover and the first order phase transition region. As shown previously, the susceptibilities for the non-interacting ideal HRG (pink dashed line) show a monotonous rising behaviour not being affected by a varied vector coupling strength.

The ratio of the fourth order to the second order coefficients in the three different regions of the phase diagram is shown in Fig. 9 for vector couplings  $r_v = 0$  in panel (a) and  $r_v = 0.9$  in panel (b). Once again, the height of the peak at the critical temperature shows a major dependence on the strength of the vector coupling. Comparing the curves of the three different regimes of the phase diagram, the susceptibilities show a significantly different slope around  $T_c$ . At non-vanishing baryochemical potentials the ratios deviate significantly from the HRG results what is similar to the findings of suppressed fluctuations in higher order cumulants in the vicinity of the transition region at zero baryochemical potential [83]. In our case the fluctuations are suppressed by the repulsive vector interactions. This fact could help to probe the location of the phase transition and a possible critical end point

experimentally by extraction of the susceptibilities from data.

However, the good agreement of our results for the susceptibilities in the crossover region given a vector coupling strength of  $r_v = 0.9$  with the lattice data for vanishing baryochemical potential (green dashed line in Fig. 9 (b)) together with the results for the chiral order parameter  $\sigma$  in the whole  $T-\mu$  plane (Fig. 2), leads us to the conclusion, that the existence of a critical end point according to our model is very questionable. The results from our model suggest that for reasonable values of the vector coupling, throughout the entire phase diagram the phase transition is a smooth crossover, ruling out the existence of a critical end point. This finding corresponds well with the results from most recent lattice data [33].

#### IV. CONCLUSIONS

We presented an effective chiral  $SU(3)$  model for the QCD equations of state. In this sigma-omega model we included all known hadrons up to resonances with masses of 2.6 GeV together with a parameter  $r_v$  that controls the coupling strength of the baryons to the repulsive vector meson field. Furthermore, we include a finite size effect that effectively suppresses heavy particles at higher densities.

Using this model, at zero baryochemical potential  $\mu_B$  we found a smooth crossover phase transition for the order parameter of the chiral condensate  $\sigma$  with a critical temperature in the range from  $T_c = 164$  MeV to  $T_c = 174$  MeV depending on the excluded volume effects being taken into account. These results are in good agreement with various data from lattice QCD. Extending this study to finite  $\mu_B$ , we show the strong dependence of the phase transition, i.e. position and order, on the vector coupling strength. For reasonable values of  $r_v$ , we find that the phase transition is a smooth crossover in the whole  $T-\mu_B$  plane and that there is no critical end point.

We also show the thermodynamic quantities from the model and calculate the quark number and strange quark number susceptibility coefficients at different values of  $\mu_B$ . The susceptibilities show a good qualitatively agreement with lattice data if a sufficiently strong vector coupling is chosen. This finding underlines the model suggestion of the non-existence of the critical end point. If the susceptibilities are extracted at different positions on the phase boundary, we show that their significantly different behavior may be used to distinguish the order of the phase transition at a given point.

#### V. ACKNOWLEDGEMENTS

This work was supported by BMBF, GSI, and by the Hessian LOEWE initiative through the Helmholtz International Center for FAIR (HIC for FAIR), and the

Helmholtz Graduate School for Hadron and Ion Research (HGS-HIRe). We are grateful to the Center for the Sci-

entific Computing (CSC) at Frankfurt University for providing the computational resources.

---

[1] I. Arsene *et al.* (BRAHMS), Nucl. Phys. **A757**, 1 (2005).  
 [2] B. B. Back *et al.*, Nucl. Phys. **A757**, 28 (2005).  
 [3] J. Adams *et al.* (STAR), Nucl. Phys. **A757**, 102 (2005).  
 [4] K. Adcox *et al.* (PHENIX), Nucl. Phys. **A757**, 184 (2005).  
 [5] M. Gyulassy and L. McLerran, Nucl. Phys. **A750**, 30 (2005).  
 [6] B. Svetitsky and L. G. Yaffe, Nucl. Phys. **B210**, 423 (1982).  
 [7] Y. Nambu and G. Jona-Lasinio, Phys. Rev. **122**, 345 (1961).  
 [8] D. A. Kirzhnits and A. D. Linde, Phys. Lett. **B42**, 471 (1972).  
 [9] S. Weinberg, Phys. Rev. **D9**, 3357 (1974).  
 [10] F. Karsch, Nucl. Phys. Proc. Suppl. **83**, 14 (2000).  
 [11] Z. Fodor and S. D. Katz, Phys. Lett. **B534**, 87 (2002).  
 [12] Z. Fodor, S. D. Katz, and K. K. Szabo, Phys. Lett. **B568**, 73 (2003).  
 [13] Z. Fodor and S. D. Katz, JHEP **04**, 050 (2004).  
 [14] F. Karsch, J. Phys. **G31**, S633 (2005).  
 [15] Y. Aoki, G. Endrodi, Z. Fodor, S. D. Katz, and K. K. Szabo, Nature **443**, 675 (2006).  
 [16] M. Cheng *et al.*, Phys. Rev. **D74**, 054507 (2006).  
 [17] M. Cheng *et al.*, Phys. Rev. **D75**, 034506 (2007).  
 [18] C. DeTar, PoS **LAT2008**, 001 (2008).  
 [19] P. Petreczky, Nucl. Phys. **A830**, 11c (2009).  
 [20] Z. Fodor and S. D. Katz, JHEP **03**, 014 (2002).  
 [21] Z. Fodor, S. D. Katz, and C. Schmidt, JHEP **03**, 121 (2007).  
 [22] C. Allton, S. Ejiri, S. Hands, O. Kaczmarek, F. Karsch, *et al.*, Phys. Rev. **D66**, 074507 (2002).  
 [23] P. de Forcrand and O. Philipsen, Nucl. Phys. **B673**, 170 (2003).  
 [24] M. D'Elia and M.-P. Lombardo, Phys. Rev. **D67**, 014505 (2003).  
 [25] M. D'Elia, F. Di Renzo, and M. P. Lombardo, Phys. Rev. **D76**, 114509 (2007).  
 [26] C. R. Allton *et al.*, Phys. Rev. **D71**, 054508 (2005).  
 [27] P. de Forcrand and O. Philipsen, JHEP **11**, 012 (2008).  
 [28] O. Kaczmarek *et al.*, Phys. Rev. **D83**, 014504 (2011).  
 [29] L.-K. Wu, X.-Q. Luo, and H.-S. Chen, Phys. Rev. **D76**, 034505 (2007).  
 [30] M. A. Stephanov, K. Rajagopal, and E. V. Shuryak, Phys. Rev. Lett. **81**, 4816 (1998).  
 [31] M. A. Stephanov, K. Rajagopal, and E. V. Shuryak, Phys. Rev. **D60**, 114028 (1999).  
 [32] M. A. Stephanov, PoS **LAT2006**, 024 (2006).  
 [33] G. Endrodi, Z. Fodor, S. Katz, and K. Szabo, JHEP **1104**, 001 (2011).  
 [34] J. D. Walecka, Annals Phys. **83**, 491 (1974).  
 [35] B. D. Serot and J. D. Walecka, Adv. Nucl. Phys. **16**, 1 (1986).  
 [36] J. Boguta and A. R. Bodmer, Nucl. Phys. **A292**, 413 (1977).  
 [37] J. Boguta and H. Stöcker, Phys. Lett. **B120**, 289 (1983).  
 [38] A. S. Khvorostukhin, V. D. Toneev, and D. N. Voskresensky, Nucl. Phys. **A791**, 180 (2007).  
 [39] A. S. Khvorostukhin, V. D. Toneev, and D. N. Voskresensky, Nucl. Phys. **A813**, 313 (2008).  
 [40] Y. Nambu and G. Jona-Lasinio, Phys. Rev. **124**, 246 (1961).  
 [41] P. Papazoglou, S. Schramm, J. Schaffner-Bielich, H. Stöcker, and W. Greiner, Phys. Rev. **C57**, 2576 (1998).  
 [42] P. Papazoglou, D. Zschiesche, S. Schramm, J. Schaffner-Bielich, H. Stöcker, *et al.*, Phys. Rev. **C59**, 411 (1999).  
 [43] F. Karsch, K. Redlich, and A. Tawfik, Eur. Phys. J. C **29**, 549 (2003).  
 [44] F. Karsch, K. Redlich, and A. Tawfik, Phys. Lett. B **571**, 67 (2003).  
 [45] P. Huovinen and P. Petreczky, (2010), arXiv:1005.0324.  
 [46] S. Borsanyi *et al.* (Wuppertal-Budapest), JHEP **1009**, 073 (2010).  
 [47] S. Borsanyi, Z. Fodor, C. Hoelbling, S. D. Katz, S. Krieg, C. Ratti, and K. K. Szabo, (2010), arXiv:1012.5215.  
 [48] M. Cheng, P. Hendge, C. Jung, F. Karsch, O. Kaczmarek, *et al.*, Phys. Rev. **D79**, 074505 (2009).  
 [49] J. Cleymans and K. Redlich, Phys. Rev. Lett. **81**, 5284 (1998).  
 [50] J. Cleymans and K. Redlich, Phys. Rev. **C60**, 054908 (1999).  
 [51] F. Becattini, J. Cleymans, A. Keranen, E. Suhonen, and K. Redlich, Phys. Rev. **C64**, 024901 (2001).  
 [52] P. Braun-Munzinger, D. Magestro, K. Redlich, and J. Stachel, Phys. Lett. **B518**, 41 (2001).  
 [53] A. Andronic, P. Braun-Munzinger, K. Redlich, and J. Stachel, Phys. Lett. **B571**, 36 (2003).  
 [54] J. Steinheimer, S. Schramm, and H. Stöcker, (2009), arXiv:0909.4421.  
 [55] J. Steinheimer, S. Schramm, and H. Stöcker, J. Phys. G **G38**, 035001 (2011).  
 [56] V. Koch, (2008), arXiv:0810.2520.  
 [57] V. Dexheimer and S. Schramm, Astrophys. J. **683**, 943 (2008).  
 [58] K. Nakamura *et al.* (Particle Data Group), J. Phys. **G37**, 075021 (2010).  
 [59] A. Mocsy, I. N. Mishustin, and P. J. Ellis, Phys. Rev. **C70**, 015204 (2004).  
 [60] E. S. Bowman and J. I. Kapusta, Phys. Rev. **C79**, 015202 (2009).  
 [61] D. Zschiesche, A. Mishra, S. Schramm, H. Stöcker, and W. Greiner, Phys. Rev. C **70**, 045202 (2004).  
 [62] D. H. Rischke, M. I. Gorenstein, H. Stöcker, and W. Greiner, Z. Phys. **C51**, 485 (1991).  
 [63] J. Baacke, Acta Phys. Polon. **B8**, 625 (1977).  
 [64] R. Hagedorn and J. Rafelski, Phys. Lett. **B97**, 136 (1980).  
 [65] M. I. Gorenstein, V. K. Petrov, and G. M. Zinovev, Phys. Lett. **B106**, 327 (1981).  
 [66] R. Hagedorn, Z. Phys. **C17**, 265 (1983).  
 [67] J. Steinheimer, S. Schramm, and H. Stöcker, Phys. Rev. **C84**, 045208 (2011).  
 [68] A. Bazavov *et al.*, Phys. Rev. **D80**, 014504 (2009).

- [69] A. Bazavov and P. Petreczky (HotQCD), J. Phys. Conf. Ser. **230**, 012014 (2010).
- [70] A. Bazavov and P. Petreczky, (2010), arXiv:1009.4914.
- [71] M. Cheng *et al.*, Phys. Rev. **D81**, 054504 (2010).
- [72] Y. Aoki, S. Borsanyi, S. Durr, Z. Fodor, S. D. Katz, *et al.*, JHEP **0906**, 088 (2009).
- [73] S. Ejiri *et al.*, Prog. Theor. Phys. Suppl. **153**, 118 (2004).
- [74] S. Borsanyi *et al.*, JHEP **11**, 077 (2010).
- [75] C. E. Detar and R. Gupta (HotQCD), PoS **LAT2007**, 179 (2007).
- [76] P. Gerber and H. Leutwyler, Nucl. Phys. **B321**, 387 (1989).
- [77] A. Mishra, S. Schramm, and W. Greiner, Phys. Rev. **C78**, 024901 (2008).
- [78] A. Bazavov and P. Petreczky, PoS **LAT2010**, 169 (2010).
- [79] C. Schmidt, PoS **CPOD2009**, 024 (2009).
- [80] F. Karsch, B.-J. Schaefer, M. Wagner, and J. Wambach, Phys. Lett. **B698**, 256 (2011).
- [81] T. Kunihiro, Phys. Lett. **B271**, 395 (1991).
- [82] J. Steinheimer and S. Schramm, Phys. Lett. **B696**, 257 (2011).
- [83] B. Friman, F. Karsch, K. Redlich, and V. Skokov, Eur. Phys. J. **C71**, 1694 (2011).